Investigation of Asymmetrically Clipped Optical Wavelet Based OFDM System

Farhad Sadeghi Almaloo, Majid Zarie, and Ghader Mohammadi Aghdash
Electrical Engineering Department, khatam al-anbia (pbuh) University, Tehran, Iran
Email: fr.sd1352@gmail.com; majidzarie@yahoo.com; aletaha.mohammadi@yahoo.com

Abstract —An Asymmetrically Clipped Optical Wavelet based Orthogonal Frequency Division Multiplexing (ACO WOFDM) system over multimode optical channel is investigated. Wavelet Packet Transform (WPT) is used to generate WOFDM symbols. Haar and Symlets wavelets are utilized to implement the WOFDM. Quadrature Amplitude Modulation (QAM) is used as the modulation format. The simulation results show that the ACO WOFDM system attains a considerable BER performance improvement over the conventional Fourier based system.

Index Terms—ACO WOFDM, ACO OFDM, haar, symlets, WPT

I. Introduction

The main advantage of Orthogonal Frequency Division Multiplexing (OFDM) is its robustness against channel dispersion. This feature makes OFDM a strong modulation technique for high speed communication systems in dispersive environments. OFDM has been proposed for dispersion compensation in optical communication systems [1]. The fundamental challenge to implement optical OFDM is converting the bipolar electrical OFDM signal to a unipolar optical signal. To this end, optical structures such as DC biased Optical (DCO) structure and Asymmetrically Clipped Optical (ACO) structure have been proposed for OFDM transmission over multimode optical fibers and free space optical channels [2]-[10]. In these structures, optical modulation format is intensity modulation in which the electrical OFDM signal is represented as the intensity of light.

The strategy of OFDM to overcome channel dispersion is simultaneous transmission of long duration symbols. To this end, the Fourier transform modulates data symbols on the amplitudes of orthogonal subcarriers, i.e. orthogonal complex exponentials, using rectangular windowing. This process generates windowed complex exponentials that each have sinc shapes with considerable side lobes in the frequency domain. This causes Inter Carrier Interference (ICI). In WOFDM, subcarriers are the scaled and shifted versions of wavelets. Wavelets are designed in such a way to have finite length in both time and frequency domain. Wavelets have pulse shaping nature, so spectrums of wavelets contain lower side lobes than OFDM. As a result, WOFDM offers higher immunity to ICI than OFDM [11]. In addition, the orthogonality of the OFDM subcarriers relies only on their frequency position, while the orthogonality of the WOFDM subcarriers relies on both time and frequency positions. As a result, WOFDM is more robust to any change in frequency, i.e. the Doppler effect, than OFDM [12]. Furthermore, the performance of WOFDM in flat fading and frequency selective fading environments has been well studied. It has been shown that WOFDM is more robust against channel dispersion than OFDM [11]-[15]. Other advantages of WOFDM over OFDM are as such: easier implementation, lower complexity, and higher flexibility. Strong advantages of WOFDM over OFDM have caused the replacement of OFDM with WOFDM in the most recent high data rates communication systems.

In this article, we investigate the transmission performance of the ACO WOFDM system over multimode optical channel.

II. ACO OFDM

Multipath channel may introduce ISI. In communication systems, the result of receiving a specific signal from different paths is known as multipath phenomenon. When the delay times of different paths are not negligible by comparison with the symbol duration time, multipath channel introduces ISI. The most effective technique to mitigate ISI is increasing symbol duration time which reduces system data rate. In this case, the delay times of different paths would be negligible compared to the symbol duration time. Consequently, multipath channel doesn't introduce ISI. OFDM provides the opportunity to eliminate ISI without decrement of system data rate. OFDM mitigates ISI by increasing symbol duration time and prevents reduction of data rate by simultaneously transmitting data symbols. To this end, increased duration symbols are modulated on the amplitudes of orthogonal subcarriers. The Fourier transform, i.e. the Inverse Discrete Fourier Transform (IDFT), is employed to modulate long duration symbols on the amplitude of orthogonal subcarriers, i.e. complex exponentials. The obtained OFDM signal is a complex time domain signal. A real time domain signal is achieved by using an IQ modulator. The block diagrams of an OFDM transmitter and an OFDM receiver are

Manuscript received March 2, 2019; revised August 6, 2019.
Corresponding author email: fr.sd1352@gmail.com.
doi:10.12720/jcm.14.9.833-838

shown in Fig. 1 and Fig. 2, respectively. In ACO OFDM, the bipolar OFDM signal is clipped at the zero level before being modulated on the intensity of light.

III. ACO WOFDM

The Wavelet Packet Transform (WPT) belongs to the family of the wavelet transform. The basis functions of the WPT are called wavelet packets. Wavelet Packets can recursively be computed using Quadrature Mirror Filter (QMF) pairs *h(n)* and *g(n)*:

$$w_{2n}(t)=\sqrt{2}\sum_{k\in Z}h(k)w_n(2t-k) \tag{1}$$

$$w_{2n+1}(t)=\sqrt{2}\sum_{k\in Z}g(k)w_n(2t-k) \tag{2}$$

in which w_n denotes the wavelet packet function, *h(n)* is the impulse response of a low pass filter and *g(n)* is the impulse response of a high pass filter. *h(n)* and *g(n)* forms a QMF pair. They should be satisfied the following condition:

$$g(n)=(-1)^n h(L-n-1) \tag{3}$$

where L is the span of the filters. The coefficients of filters h and g are calculated by using the following equations:

$$\varphi(t)=\sum_n h(n)\sqrt{2}\varphi(2t-n), \qquad n\in Z \tag{4}$$

$$\psi(t)=\sum_n g(n)\sqrt{2}\varphi(2t-n), \qquad n\in Z \tag{5}$$

In the above equations, $\psi(t)$ and $\varphi(t)$ denote the wavelet function and the scaling function, respectively.

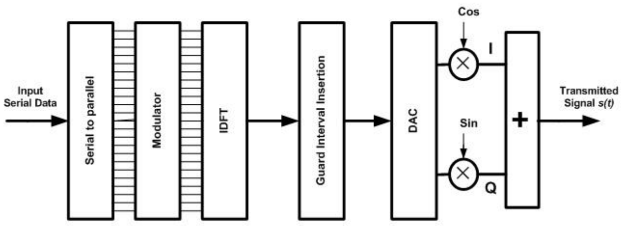

Fig. 1. Block diagram for an OFDM transmitter.

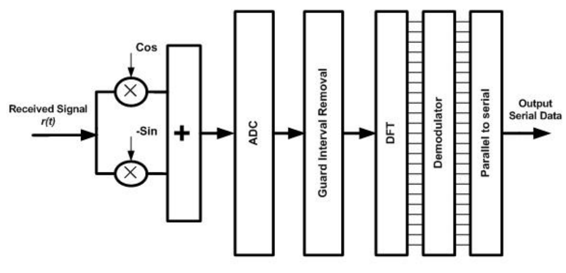

Fig. 2. Block diagram for an OFDM receiver.

Implementation of the WPT can be divided into three main steps. The first step is selecting the mother wavelet, which is known by its wavelet and scaling functions. The next step is calculating the coefficients of filters h and g. Lastly, the WPT can be constructed using multistage QMF banks. As depicted in Fig. 3 and Fig. 4, the WPT and the Inverse WPT (IWPT) are implemented using tree structures. In Fig. 3, the WPT is obtained through low pass and high pass filtering of the discrete time domain signal. Fig 4. Shows the reconstruction of the original signal from the wavelet packet coefficients or the IWPT.

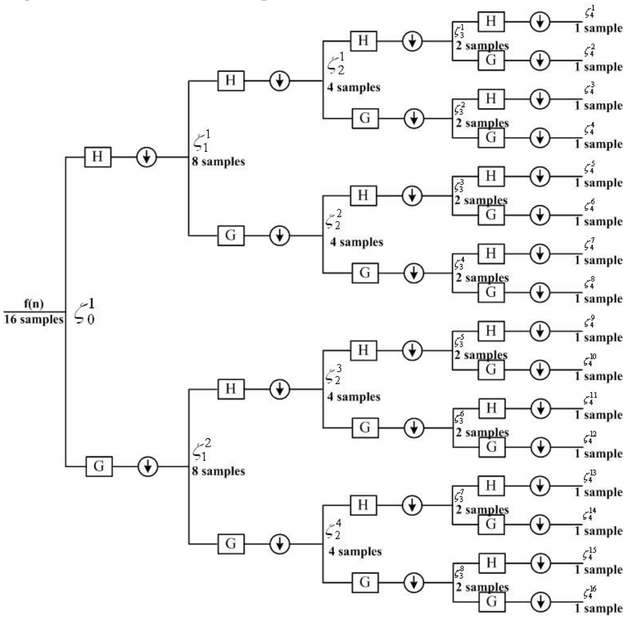

Fig. 3. A 4-stage WPT.

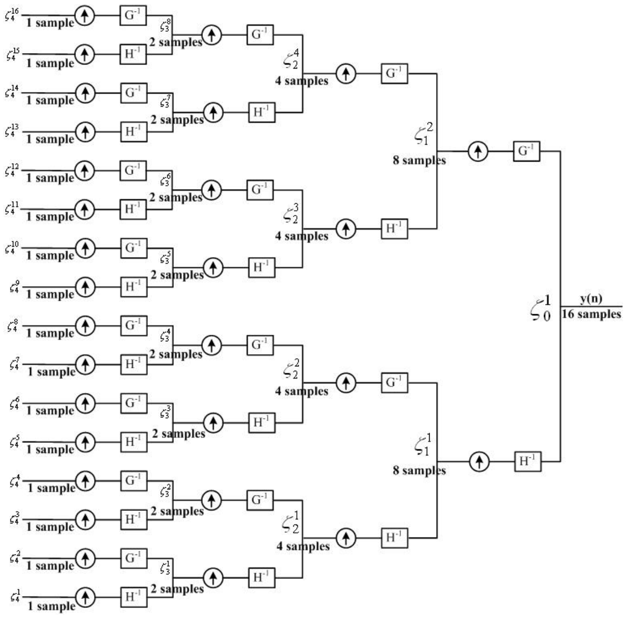

Fig. 4. A 4-stage IWPT.

The principle of WOFDM, i.e. WPT based OFDM, is very similar to the principle of conventional OFDM, i.e. Fourier transform based OFDM. OFDM utilizes Fourier transform to perform modulation and demodulation processes while WOFDM utilizes WPT to implement modulation and demodulation. In WOFDM, the IWPT is employed to carry out data modulation and the demodulation process is performed using the WPT. Number of subcarriers is determined by the number of stages in filtering processes, i.e. *number of subcarriers* = $2^{\text{number of stages}}$. For example, Fig. 4 shows a 4-stage or a 16-subcarrier WOFDM modulation system.

ACO WOFDM signal is obtained by clipping the WOFDM signal at the zero level and modulating the unipolar signal on the intensity of light.

IV. Mother Wavelets

In this section, we introduce the various mother wavelets and present their properties.

A. Haar Wavelet

Haar wavelet was the first mother wavelet proposed by Alfred Haar [16]. It is the fast and simplest wavelet. The Haar wavelet is not continuous. Therefore, it is not differentiable. This property makes it suitable for the analysis of signals with sudden transitions. The Haar wavelet function is defined as:

$$\psi(t)=\begin{cases}1 & 0<t\le 1/2\\ -1 & 1/2<t\le 1\\ 0 & elsewhere\end{cases} \tag{6}$$

It's scaling function is a rectangular pulse satisfying the following:

$$\varphi(t)=\begin{cases}1 & 0\le t\le 1\\ 0 & elsewhere\end{cases} \tag{7}$$

B. Meyer Wavelet

The Meyer wavelet is proposed by Yves Meyer [16]. Unlike the Haar wavelet, it is continuous and differentiable. The Mayer wavelet function is defined in frequency domain:

$$\Psi(w)=\begin{cases}\frac{1}{\sqrt{2\pi}}\sin\left(\frac{\pi}{2}v(\frac{3|w|}{2\pi}-1)\right)e^{\frac{jw}{2}} & \frac{2\pi}{3}\le|w|\le\frac{4\pi}{3}\\ \frac{1}{\sqrt{2\pi}}\cos\left(\frac{\pi}{2}v(\frac{3|w|}{4\pi}-1)\right)e^{\frac{jw}{2}} & \frac{4\pi}{3}\le|w|\le\frac{8\pi}{3}\\ 0 & elsewhere\end{cases} \tag{8}$$

where, v is a smooth function.

$$v(x)=\begin{cases}0 & x<0\\ x & 0\le x\le 1\\ 1 & x>1\end{cases} \tag{9}$$

The Mayer scaling function in frequency domain is given by:

$$\Phi(w)=\begin{cases}\frac{1}{\sqrt{2\pi}} & |w|\le\frac{2\pi}{3}\\ \frac{1}{\sqrt{2\pi}}\cos\left(\frac{\pi}{2}v(\frac{3|w|}{2\pi}-1)\right) & \frac{2\pi}{3}\le|w|\le\frac{4\pi}{3}\\ 0 & elsewhere\end{cases} \tag{10}$$

The Meyer wavelet and scaling functions are plotted in Fig. 5 and Fig. 6, respectively.

C. Morlet Wavelet

The Morlet wavelet function is a complex exponential multiplied by a Gaussian window; therefore, its spectrum is a shifted Gaussian [16]. The Morlet wavelet function can be described by

$$\psi(t)=e^{-jw_0t}e^{-t^2/2} \tag{11}$$

Fig. 7 shows real part of the Morlet wavelet for $w_0=5$.

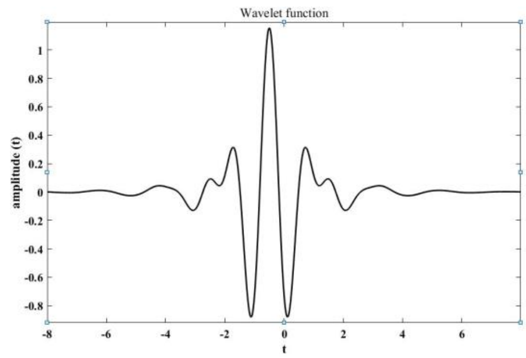

Fig. 5. The Meyer wavelet function in time domain.

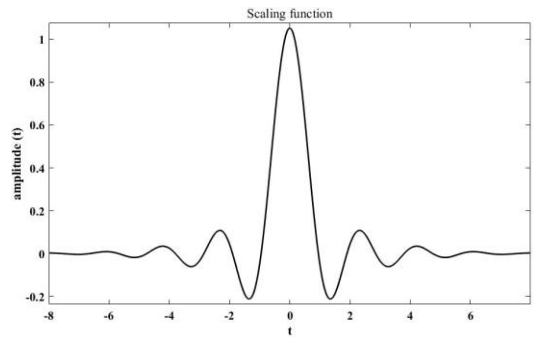

Fig. 6. The Meyer scaling function in time domain.

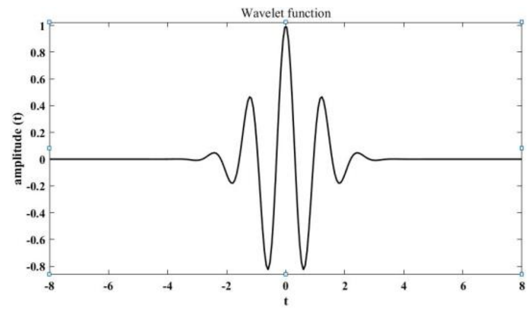

Fig. 7. Real part of the Morlet wavelet function.

D. Daubechies Wavelet

The Daubechies wavelet has two special properties. It is a type of orthogonal wavelets. Its wavelet and scaling functions have compact support [16]. The Daubechies wavelet and scaling functions are depicted in Fig. 8 and Fig. 9, respectively.

E. Symlets Wavelet

The Symlets wavelets are modified versions of Daubechies. They are nearly symmetrical wavelets and very compactly supported.

V. Simulation and Discussion

Fig. 10 shows the simulation models of the ACO WOFDM and ACO OFDM systems. At the transmitter, a parallel to serial convertor is employed to generate parallel data. Next, each parallel data channel is mapped onto 16-ary Quadrature Amplitude Modulation (QAM) symbol. The information symbols are then transformed into a complex time domain samples via an IWPT. Guard Interval (GI) insertion is performed. GI acts as a space between successive WOFDM symbols and therefore prevents ISI. A real time passband WOFDM signal is obtained through a DAC and an IQ modulator. The negative parts of the signal are clipped off. The signal is modulated on the intensity of light using an optical modulator, i.e. Mach Zehnder Modulator (MZM). Receiver, performs the reverse operations of the transmission scheme to recover the original data.

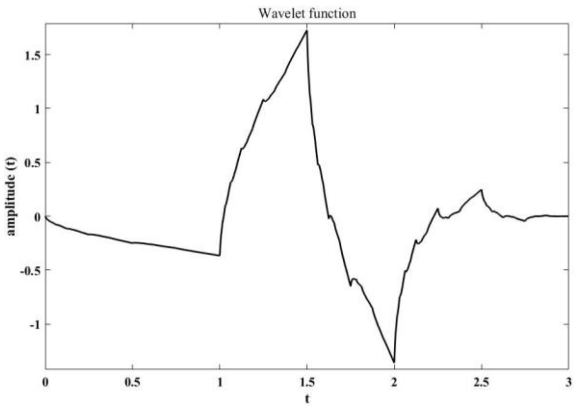

Fig. 8. The Daubechies wavelet function.

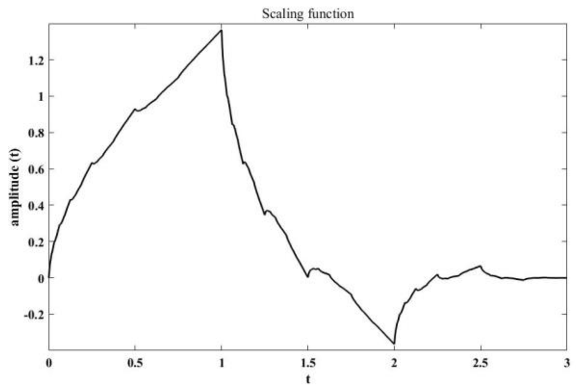

Fig. 9. The Daubechies scaling function.

Table I lists simulation parameters. Optisystem is used to carry out simulations. The optical power of the transmitter laser is 0dBm. The wavelength and the linewidth of the laser beam are 850 nm and 10 MHz, respectively. The modal bandwidth of the multimode fiber is 1324 MHz.km and the loss of the fiber is 2.61 dB/km. A PIN photodetector with the dark current of 10 nA and Responsivity of 1 A/W is utilized to receive the optical signal.

The received constellations are depicted in Fig. 11 and Fig. 12. It is evident that the high frequency components of the ACO OFDM signal is more attenuated than the high frequency component of the ACO WOFDM signal. This implies that the spectrum of the ACO WOFDM signal is more compatible with the channel frequency response than the spectrum of the ACO OFDM signal.

BER and OSNR diagrams are shown in Fig. 13 and Fig. 14, respectively. A considerable improvement in BER performance of the ACO WOFDM systems can be seen compared to the ACO OFDM system. It is clear that, the Symlets based scheme works better than the Haar based WOFDM.

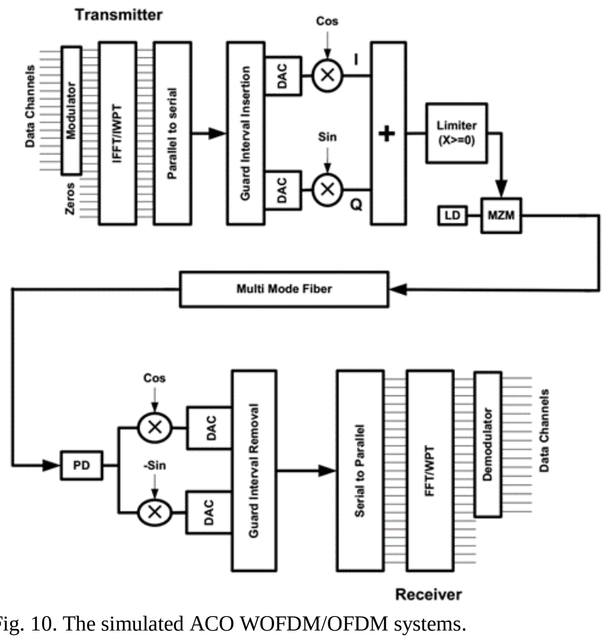

Fig. 10. The simulated ACO WOFDM/OFDM systems.

TABLE I: SIMULATION PARAMETERS

	OFDM	WPT-OFDM
Parameter	**Value**	**Value**
Carrier frequency	15 GHz	15 GHz
Data rate	10 Gb/s	10 Gb/s
Baseband bandwidth	2.5 GHz	1.25 GHz
Modulation	16-QAM	16-QAM
Transmitted symbols	28	28
Transmitted bits	28784	28784
WPT/FFT points	1024	1024
Subcarriers	1024	1024
Cyclic prefix	128	128
Mother Wavelet	----	Haar, Symlets2

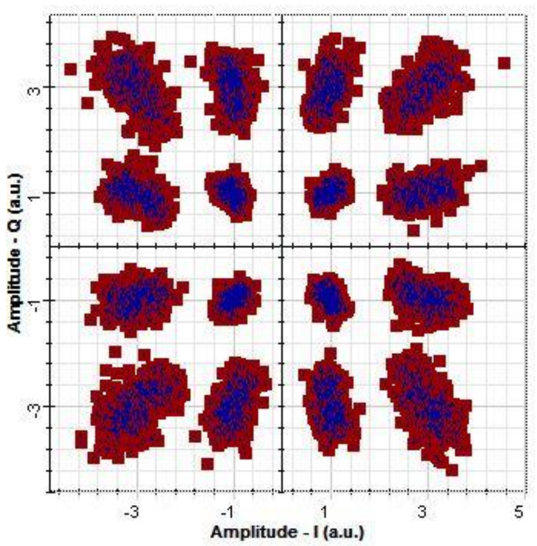

Fig. 11. The received constellations of OFDM symbols after transmitting 135 m.

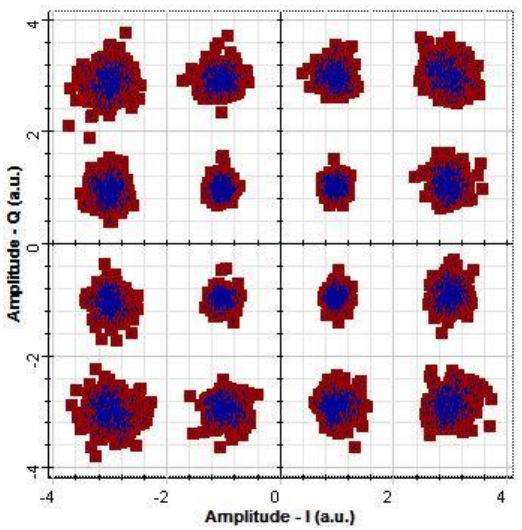

Fig. 12. The received constellations of WOFDM symbols after transmitting 135 m.

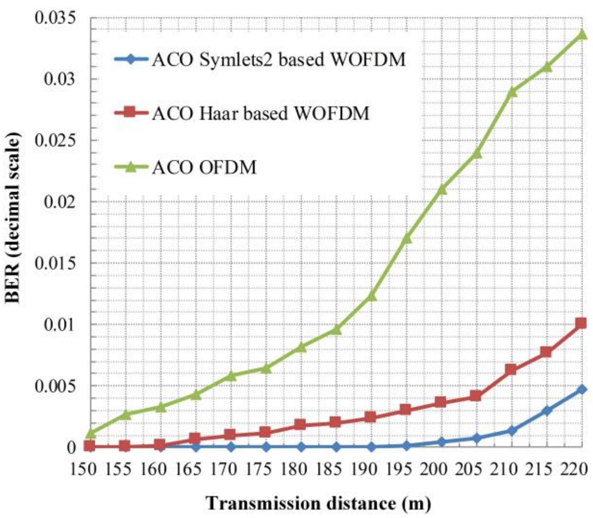

Fig. 13. BER versus transmission distance.

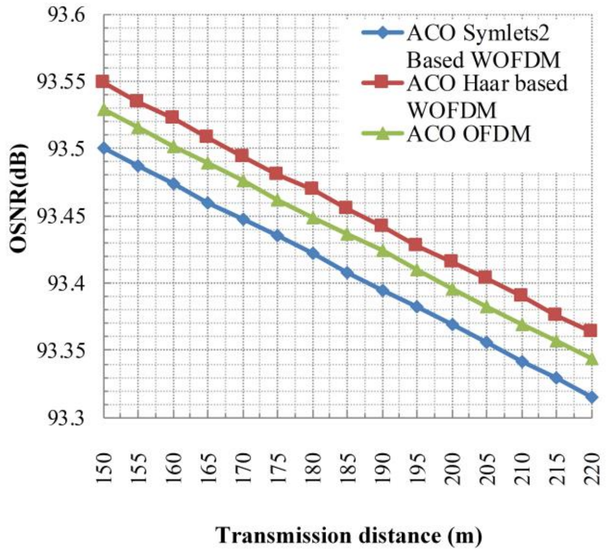

Fig. 14. OSNR versus transmission distance.

VI. Conclusions

The BER performance of the ACO WOFDM system in multimode optical fiber has been investigated. It was found that the ACO WOFDM system offers substantial advantages over the conventional Fourier based system.

References

[1] J. Armstrong, "OFDM for optical communications," *Journal of Lightwave Technology*, vol. 27, no. 3, pp. 189-204, Feb. 2009.

[2] A. Mirbadin and A. B. Mohammad, "Performance analysis of DCO OFDM and DCO WOFDM systems in MMF optical links," in *Proc. IEEE Pacific Rim Conference on Communications, Computers and Signal Processing*, Victoria, BC, 2011, pp. 388-393.

[3] N. Yin, C. Guo, Y. Yang, P. Luo, and C. Feng, "Asymmetrical and direct current biased optical OFDM for visible light communication with dimming control," in *Proc. IEEE International Conference on Communications Workshops (ICC Workshops)*, Paris, 2017, pp. 23-28.

[4] M. M. A. Mohammed, C. He, and J. Armstrong, "Diversity combining in layered asymmetrically clipped optical OFDM," *Journal of Lightwave Technology*, vol. 35, no. 11, pp. 2078-2085, Jun. 2017.

[5] X. Zhang, Q. Wang, R. Zhang, S. Chen, and L. Hanzo, "Performance analysis of layered ACO-OFDM," *IEEE Access*, vol. 5, pp. 18366-18381, Aug. 2017.

[6] W. Xu, M. Wu, H. Zhang, X. You, and C. Zhao, "ACO-OFDM-Specified recoverable upper clipping with efficient detection for optical wireless communications," *IEEE Photonics Journal*, vol. 6, no. 5, pp. 1-17, Oct. 2014.

[7] Y. Yang, Z. Zeng, J. Cheng, and C. Guo, "An enhanced DCO-OFDM scheme for dimming control in visible light communication systems," *IEEE Photonics Journal*, vol. 8, no. 3, pp. 1-13, Jun. 2016.

[8] X. Zhang, P. Liu, J. Liu, and S. Liu, "Advanced A-law employing nonlinear distortion reduction in DCO-OFDM systems," in *Proc. IEEE/CIC International Conference on*

Communications in China - Workshops (CIC/ICCC), Shenzhen, 2015, pp. 184-188.
[9] A. A. Abdulkafi, M. Y. Alias, and Y. S. Hussein, "Performance analysis of DCO-OFDM in VLC system," in *Proc. IEEE 12th Malaysia International Conference on Communications (MICC)*, Kuching, 2015, pp. 163-168.
[10] M. Jiang, J. Zhang, X. Liang, and C. Zhao, "Direct current bias optimization of the LDPC Coded DCO-OFDM systems," *IEEE Photonics Technology Letters*, vol. 27, no. 19, pp. 2095-2098, Oct. 2015.
[11] M. Oltean and M. Nafornita, "Efficient pulse shaping and robust data transmission using wavelets," in *Proc. IEEE International Symposium on Intelligent Signal Processing*, Alcala de Henares, 2007, pp. 1-6.
[12] M. Oltean and M. Nafornita, "Errors per scale statistics for a wavelet OFDM transmission in flat fading channels," in *Proc. IEEE International Symposium on Intelligent Signal Processing*, Budapest, 2009, pp. 119-124.
[13] H. C. Yu, Y. R. Chien, and H. W. Tsao, "A study of impulsive noise immunity for wavelet-OFDM-based power line communications," in *Proc. International Conference On Communication Problem-Solving (ICCP)*, Taipei, 2016, pp. 1-2.
[14] M. Chafii, J. Palicot, R. Gribonval, and A. G. Burr, "Power spectral density limitations of the wavelet-OFDM system," in *Proc. 24th European Signal Processing Conference (EUSIPCO)*, Budapest, 2016, pp. 1428-1432.
[15] M. Chafii, Y. J. Harbi, and A. G. Burr, "Wavelet-OFDM vs. OFDM: Performance comparison," in *Proc. 23rd International Conference on Telecommunications (ICT)*, Thessaloniki, 2016, pp. 1-5.
[16] M. Vetterli and J. Kovacevic, *Wavelets and Subband Coding*, New Jersey: Prentice Hall, 2007, pp. 209-325.

Farhad Sadeghi Almaloo was born in Tehran, Iran. He received the B.S. degree from the Air University, Tehran, Iran, in 1998 and the M.S. degree from the Imam Hossein Comprehensive University, Tehran, Iran, in 2012, both in communication engineering. He is currently pursuing the Ph.D. degree at the Islamic Azad University, Science and Research Branch, Tehran, Iran. He is at present working as instructor in the khatam al-anbia(pbuh) University, Tehran, Iran His research interests include optical communications, coding theory, digital signal processing, digital image processing, and pattern recognition.

Majid Zarie received his bachelor's degree in Electrical-Electronics Engineering from the Shahid Rajaee Teacher Training University, Tehran, Iran and his Master's degree in Electrical-Electronics Engineering from the Imam Hossein Comprehensive University, Tehran, Iran. He received his Ph.D degree in Electrical-Electronics Engineering from the Malek Ashtar University of Technology, Tehran, Iran. He is at present working as assistant professor in the khatam al-anbia(pbuh) University, Tehran, Iran. His current research interests are optical communications, digital signal processing, and digital image processing.

Ghader Mohammadi Aghdash received his bachelor's degree in Electrical-Electronics Engineering from the Shahid Rajaee Teacher Training University, Tehran, Iran and his Master's degree in Electrical-Electronics Engineering from the Islamic Azad University, Science and Research Branch, Tehran, Iran. He is at present working as instructor in the khatam al-anbia(pbuh) University, Tehran, Iran. His current research interests are optical communications, digital signal processing, and digital image processing.